

Effect of prolactin on cytotoxicity and oxidative stress in ovine ovarian granulosa cells

Ruochen Yang^{1,*}, Shuo Zhang^{2,*}, Chunhui Duan¹, Yunxia Guo¹, Xinyu Shan¹, Xinyan Zhang¹, Sicong Yue¹, Yingjie Zhang¹ and Yueqin Liu¹

¹ Hebei Agricultural University, Baoding, China

² China Agricultural University, Beijing, China

* These authors contributed equally to this work.

ABSTRACT

Background. Prolactin (PRL) has been reported to be associated with oxidative stress, which is an important contributor leading to cell apoptosis. However, little is known about the mechanisms underlying the effects of PRL on cytotoxicity and oxidative stress in ovine ovarian granulosa cells (GCs).

Methods. Ovine ovarian GCs were treated with 0, 4, 20, 100 and 500 ng/mL of PRL. Then, the cytotoxicity, cell viability, malondialdehyde (MDA), reactive oxygen species (ROS), superoxide dismutase (SOD) and total antioxidant capacity (T-AOC) of GCs were detected. Additionally, 500 ng/mL PRL was chosen as the high PRL concentration (HPC) due to its high cytotoxicity and oxidative stress. Proteomic and metabolomic were performed to examine the overall difference in proteins and metabolic pathways between C (control: 0 ng/mL PRL) and P groups (500 ng/mL PRL).

Results. The results indicated that GCs treated with 4 ng/mL PRL significantly decreased ($P < 0.05$) the cytotoxicity, ROS and MDA, increased ($P < 0.05$) the cell viability, SOD and T-AOC, and the GCs treated with 500 ng/mL PRL showed the opposite trend ($P < 0.05$). Supplementation with 500 ng/mL PRL significantly increased the proteins of MT-ND1, MAPK12, UBA52 and BCL2L1, which were enriched in ROS and mitophagy pathways. Pathway enrichment analysis showed that the pentose phosphate pathway was significantly enriched in the P group.

Conclusion. A low concentration of PRL inhibited cytotoxicity and oxidative stress. HPC induced oxidative stress in ovine ovarian GCs via the pentose phosphate pathway by modulating the associated proteins MT-ND1 in ROS pathway and UBA52, MAPK12 and BCL2L1 in mitophagy pathway, resulting in cytotoxicity.

Subjects Biochemistry, Cell Biology, Toxicology

Keywords Ovine, PRL, GCs, Cytotoxicity, Oxidative Stress

INTRODUCTION

Oxidative stress is defined as an excessive level of intracellular reactive oxygen species (ROS) production due to the imbalance between oxidation and antioxidant. ROSs includes superoxide anion ($O_2^{\cdot-}$), hydrogen peroxide (H_2O_2), and hydroxyl radicals ($-OH\cdot$), which can be scavenged by antioxidants (*Schieber & Chandel, 2014*). It has been proposed that oxidative stress can impede the reproduction function of the body (*Meniri et al.,*

Submitted 8 March 2023

Accepted 2 June 2023

Published 10 July 2023

Corresponding authors

Yingjie Zhang,

zhangyingjie66@126.com

Yueqin Liu, liuyueqin66@126.com

Academic editor

Sonia Oliveira

Additional Information and
Declarations can be found on
page 18

DOI 10.7717/peerj.15629

© Copyright
2023 Yang et al.

Distributed under
Creative Commons CC-BY 4.0

OPEN ACCESS

2022). A study by *Stier et al. (2012)* indicated that pre-reproductive oxidative damage was significantly related to mice's litter size at birth. The oxidative stress generated at high altitudes or under low air pressure can affect the development and function of the sheep corpus luteum, further leading to reduced fertility (*Parraguez et al., 2013*). The ROS and O^{2-} radicals may be involved in human reproduction (*Drejza et al., 2022; Veena et al., 2008*), while oxidative stress is the most frequent cause of female infertility disorders, including polycystic ovary syndrome (PCOS) (*Mohammadi, 2019*). Additionally, previous studies have demonstrated the critical physiological role of ROS, which was locally produced by endothelial cells, neutrophils and macrophages within the follicle during folliculogenesis and ovulation (*Mitchell & Johnston, 2022; Abedelahi et al., 2010; Hennet, Yu & Combelles, 2013*). *In vitro*, plenty of evidence showed that oxidative stress is responsible for the abnormal growth and function of granulosa cells (GCs) during ovarian follicular development (*Zhang et al., 2016a; Zhang et al., 2016b; Li et al., 2016*). Subsequently, GCs apoptosis leads to follicular atresia (*Yuan et al., 2016*) and, more seriously, oocyte and ovarian dysfunction (*Lai et al., 2018*).

Prolactin (PRL) is a protein hormone synthesized and secreted by several cells and tissues in the body, such as anterior pituitary, mammary glands, T-lymphocytes and hypothalamus (*Henriques et al., 2022*). The normal serum PRL levels in females, depending on reference values, range from nearly 2 to 25 ng/mL (average 13 ng/ml) (*Melmed et al., 2011*). But the chemical immunoassay showed that the serum PRL levels of females (*Table 1*) were different in different periods (*Lu et al., 1983*). PRL in follicular fluid was always found to be at a higher concentration than in serum (*Kamel et al., 1994*). A previous study has shown that the normal content of PRL in small follicles (<eight mm) is 35.42 ± 3.63 ng/ml, significantly higher than that in large follicles with 24.53 ± 2.50 ng/ml PRL (*Gu et al., 1993*). The normal serum concentrations of PRL in ewes ranged between 12 and 24 ng/mL (17.8 ± 1.5 ng/mL, on average) (*Caja et al., 2020*). A previous study has shown that 10 ng/mL PRL can promote endothelial cell proliferation and capillary formation (*Malaguarnera et al., 2002*), whereas 2 μ M PRL dramatically increased the NK-mediated killing of the K562 cell line (*Mavoungou, Bouyou-Akotet & Kremsner, 2005*), indicating that low concentrations of PRL promote cell proliferation, but high concentrations increase cytotoxicity. Some studies also emphasized that different doses of PRL can alter oxidative-antioxidant balance in mammals (*Farmer, Lapointe & Cormier, 2017; Rodak et al., 2022*). *Thebanlt (2017)* showed that PRL helps the retinal pigment epithelium to survive *via* antioxidant actions, while *Rodak et al. (2022)* found that treatment with 300 ng/mL of PRL induced oxidative stress in human MIN6 cells. PRL excess (hyperprolactinemia) may lead to hypogonadism, which can aggravate the oxidative stress in the body (*Veena et al., 2008*). Meanwhile, a previous study has reported that higher PRL concentration can generate reproductive disorders by inducing oxidative stress and damage (*Veena et al., 2008; Hilali et al., 2013*). At the same time, females with endocrine abnormalities also have high PRL levels in the blood, creating hyperprolactinemia, which causes insufficient ovarian function, overflowing milk, and in severe cases, affecting follicle growth (*Chen, Fu & Huang, 2016*). Therefore, the influence of high PRL concentrations on cellular oxidative stress and physiological functions require more attention.

Table 1 The serum PRL levels of females was different in different periods.

Item	Periods				
	Follicular phase	Luteal phase	Pregnancy (1–3 months)	Pregnancy (4–6 months)	Pregnancy (7–9 months)
PRL (ng/mL)	17.30 ± 2.31	21.18 ± 3.29	47 ± 9.1	104 ± 2.2	348 ± 33.3

In this study, we investigated the impact of varied concentrations of PRL on GCs cytotoxicity and oxidative stress, intending to establish a theoretical foundation for enhancing GCs growth and addressing functional irregularities. It will provide a basis for future applications of PRL in ruminant reproduction.

MATERIAL AND METHODS

Cell collection

Abnormal follicle development can lead to decreased fecundity of sheep and affect production (Zhang *et al.*, 2016a; Zhang *et al.*, 2016b; Li *et al.*, 2016). At the same time, it is also believed that the dysfunction of granulosa membrane cells caused by high concentration of PRL reduces the production of steroid hormones in ovary, which affects the development and maturation of follicles, leading to abnormal menstruation and ovulation disorders and infertility. Therefore, we choose sheep as the model to lay the foundation for the future application of PRL in ruminant reproduction and to provide a theoretical basis for the impact of PRL on human reproduction.

Fresh ovaries from twelve sexually mature ewes aged between 1 and 1.5 years were collected at the local cooperative abattoir (Baoding, Hebei, China), kept at 37 °C, then transported to the laboratory in a buffered saline solution supplemented with streptomycin/penicillin mixture (1%). Dominant follicles with 3–7 mm diameter were isolated from the ovaries after 3 times sterile Dulbecco's Phosphate Buffered Saline (DPBS) cleaning. Then GCs were collected from the interior of the follicles with a one mL injector and filtered with a 100 mm filter. The filtrated liquid was centrifuged at 1,500 rpm for 10 min to obtain the precipitate. Then the precipitate was lysed in one mL sterile red blood cell (RBC) lysate for 3 min to dissolve the RBC. Harvested cells were washed with DPBS \geq 3 times and used for *in vitro* culture. The growth of GCs was observed under a microscope, and non-adherent cells were removed. All procedures used in this study were approved by the Laboratory Animal Ethics Committee of Hebei Agricultural University (Hebei, P.R. China; permit number 2023045).

Cytotoxicity and cell viability assay

The GCs were seeded in 6-well-culture plates at a density of 6×10^4 per well and treated with 0, 4, 20, 100 and 500 ng/mL PRL (PROSPEC, cyt-240, purity \geq 99.0%) for 24 h to validate the toxicity of PRL. The morphology of GCs was observed by inverted phase contrast microscope to evaluate the cytotoxicity with different concentrations of PRL (normal ovarian GCs are usually spindle-shaped, while the shape changes when the external environment changes).

The direct cytotoxicity of materials was evaluated as percentage cell viability ([Troiano et al., 2018](#)) using the Cell Counting Kit 8 assay (CCK-8, ck-04; DOJINDO Laboratories, Munich, Germany). GCs were seeded in 96-well-culture plates at a density of 5×10^3 per well and treated with 0, 4, 20, 100 and 500 ng/mL PRL for 24 h, respectively. Then a 10 μ L CCK-8 was added into each well, and the cells were hatched in the dark for 1-4 h. A microplate reader was used to quantify the optical density of the cells at 450 nm. Cell viability values were calculated based on test data. Cell survival rate γ calculation common formula is $\gamma = [(As-Ab)/(Ac-Ab)] \times 100\%$ (As: Optical density of P group, Ac: Optical density of C group, Ab: Optical density of the blank well).

Oxidative stress index detection

Oxidative stress assay

GCs incubated with 0, 4, 20, 100 and 500 ng/mL PRL were cultured in a 6-well plate at a density of 6×10^4 per well and then trypsinized and collected in 1.5 ml centrifuge tubes. After incubation, cells were immediately centrifuged twice at $1000 \times g$ for 10 min to remove the supernatant to obtain GCs, which were kept at -80°C prior to analysis.

Superoxide dismutase (SOD) activity (A001-3; Nanjing Jiancheng Bioengineering Institute, Jiangsu, China), malondialdehyde (MDA, Nanjing Jiancheng Bioengineering Institute, A003-1) and total antioxidant capacity (T-AOC) (A015-3-1, Nanjing Jiancheng Bioengineering Institute, Jiangsu, China) were measured following the manufacturer's instructions with respective analytical kits.

ROS detection

GCs incubated with 0, 4, 20, 100 and 500 ng/mL PRL were cultured in a 96-well plate at a density of 5×10^3 per well and then incubated with fluorescent probe of ROS (H2DCF-DA, Ex/Em = 488/525 nm) for 20 min in dark at 37°C . Then, incubated cells were washed twice with DMEM/F12 and images were captured under an inverted fluorescence microscope (Leica DM IRB, Leica, Wetzlar, Germany) using a green-fluorescence filter and images were analyzed using ImageJ 1.48v (National Institutes of Health, Bethesda, MD, USA).

Experimental design

The GCs model of PRL

In the present study, we found that cells treated with 500 ng/ml PRL showed significantly lower cell viability and higher cytotoxicity and oxidative stress than other groups. By taking into account the results of prior investigations ([Neradugomma, Subramaniam & Tawfik, 2014](#)), the concentration of 500 ng/mL PRL was selected as the model for the subsequent effects of high concentrations of prolactin (HPC) on cytotoxicity and oxidative stress in ovarian GCs. Moreover, a serum PRL level greater than 500 ng/mL is diagnostic of a macroprolactinoma ([Vilar et al., 2008](#)). Then, the GCs were treated with 0 ng/mL (C group) and 500 ng/mL ovine PRL (P group), with 6 replicates in each group. The mechanism of HPC regulating oxidative stress in ovine ovarian GCs was studied using integrated proteomic and metabolomic approaches.

Sample collection

GCs in 6-well plates from C and P groups were collected according to previously described methods (Yao, Xiao & Zhou, 2021).

Proteomic analysis

Protein extraction

Samples were shredded with liquid nitrogen, lysed in 8 M urea lysis solution, and then stored on ice for 1 h, followed by sonication for 5 min. The lysate was centrifuged for one hour at $12,000 \times g$ and 4°C . The supernatant was transferred to a clean tube. The Bradford protein test was used to determine protein concentration. Each sample's extracts were reduced with 5 mM DTT at 56°C for 25 min before being alkylated by supplementation of 14 mM Iodoacetamide at room temperature for 30 min in the dark. The urea concentration from each sample, containing 2 M at less, was digested with Tyrisin at 1:100 enzyme-to-substrate ratio and digested at 37°C for 16–18 h.

TMT labeling of peptides and HPLC fractionation

Desalted peptides were labelled using TMT6/10-plex reagents (TMT6/10 plex Isobaric Label Reagent Set, Thermo Fisher Scientific, Waltham, MA, USA) by the instructions. The labelling reagents were dissolved in acetonitrile. The differently labelled peptides were homogeneously mixed and incubated for 2 h and then desalted using a peptide desalting spin column (Thermo Fisher Scientific, Waltham, MA, USA).

TMT-labelled peptide mix was fractionated using a C18 column (Waters BEH C18 300 $\mu\text{m} \times 150 \text{ mm}$, $1.7 \mu\text{m}$) on a Rigol L3000 HPLC. The operation was as follows: mobile phases A (20 mM ammonium formate, adjusted pH to 10.0) and B (100% acetonitrile) was used to develop a gradient elution. The solvent gradient was 3%–41% acetonitrile. And 20 components were collected after separation, which were concentrated into peptide powder by vacuum and stored at -20°C .

LC-MS/MS analysis

The present research employed EASY-nLC 1200 system (Thermo Fisher Scientific, Waltham, MA, USA) and Orbitrap Q Exactive HF-X mass spectrometer (Thermo Fisher Scientific, Waltham, MA, USA) to analyze the proteomics. The peptides were separated on a homemade analytical column with a linear gradient from 5% to 100% of eluent B (0.1% FA) using TMT-6 plex at a flow rate of 300 NL/min for eluent A (0.1% FA in water). The gradient of solvent was as follows: 3–5 percent of B, 5 s; 5–15 percent of B, 23 mins 55 s; 15–28 percent of B, 21 mins; 28–38 percent of B, 7 mins 30 s; 38–100 percent of B, 5 s; 100 percent of B, 12 mins 25 s.

Data analysis

LC-MS/MS raw files were processed using Maxquant (v1.6.14) software for database search (Uniprot-sheep-proteome_UP000002356), building the database with the DDA method. Alkylation of cysteine was set as a fixed modification. Methionine oxidation and N-terminal acetylation of protein were set as a variable modification. The false discovery rate (FDR) of proteins and peptides was set at 0.01.

Different expression proteins (DEPs) were sifted by P value <0.05 and $FC >1.2$ or $FC <0.83$ [fold change, FC]. The function of DEPs was determined by gene ontology (GO) analysis through GoPlot (v1.0.2) and GO enrichment analysis of DEPs was performed from biological process (BP), molecular function (MF) and cellular component (CC). Then, the molecular process pathways for differential protein enrichment were obtained through the Kyoto Encyclopedia of Genes and Genomes (KEGG) database.

Western blotting

Total proteins from C and P groups were lysed for 30 min using phenylmethanesulfonyl fluoride (PMSF) and separated with 10% sodium dodecyl sulfate-polyacrylamide gel electrophoresis (SDS-PAGE). After that, membranes were subjected to a standard blocking with 5% non-fat milk, hybridized with primary antibody (MAPK12, 1:500, 22665-1-AP; BCL2L1, 1:1000, [R23529](#); UBA52, 1:500, 16432; MT-ND1, 1:500, A8035; GAPDH, 1:5000, 200306-7E4) at 4 °C overnight, and incubated with secondary antibody (goat anti-rabbit IgG, 1:500) at room temperature for 1 h. ImageJ software was used for grayscale analysis.

Metabolomic analysis

Metabolite extraction

First, 400 μ l prechilled methanol-acetonitrile (3:1, v/v) used to be delivered to the GCs samples of C and P groups, and the samples were homogenized with the usage of a grinding mill after standing for 1 h. The extract was centrifuged at $3,000 \times g$ for 15 min at 4 °C to obtain 400 μ l supernatant, which was dried thoroughly. Next, the samples supplementation with 100 μ l prechilled methanol-water (1:1, v/v), then the suspension was eddied (2,000 rmp, 4 °C, 3 min) and centrifuged (12,000 g, 4 °C, 10 min), to collect the supernatant for further analysis.

LC-MS/MS analysis

LC-MS/MS analyses were conducted using Vanquish UHPLC system (Thermo Fisher Scientific, Waltham, MA, USA) with an Orbitrap Q Exactive HF-X mass spectrometer (Thermo Fisher Scientific, Waltham, MA, USA). Using a linear gradient, samples were injected into a ACQUITY UPLC HSS T3 (1.7 μ m, 2.1 mm \times 150 mm) column. The LC mobile phases A (5 mM ammonium formate), B (acetonitrile), C (0.1% formic acid) and D (0.1% formic acid acetonitrile) were used. The solvent gradient was set as follows: 2% B, 1 min; 2–50% B, 8 mins; 50–98% B, 3 mins; 98% B, 1.5 mins, 98–2% B, 1.5 mins and 2% B, 3 mins for the negative polarity mode. 2% D, 1 min; 2–50% D, 8 mins; 50–98% D, 3 mins; 98% D, 1.5 mins, 98–2% D, 1.5 mins and 2% D, 3 mins for the positive polarity mode. Q Exactive HF-X mass spectrometer was operated in positive/negative polarity mode with a spray voltage of 2.5 kV, capillary temperature of 325 °C, auxiliary temperature of 300 °C, sheath gas flow rate of 30 arb and aux gas flow rate of 10 arb.

Data analysis

Peak alignment, peak picking and quantitative analysis of raw data were performed by Compound Discoverer 3.0 (CD 3.0, Thermo Fisher Scientific, Waltham, MA, USA). The main parameters were set as to the methods described previously ([He et al., 2021](#)).

In LC-MS metabolomic analysis, the following criteria were employed for selecting the differentially expressed metabolites (DEMs) in C and P groups: variable influence on projection (VIP) value >1.0 , P value <0.05 and $|FC|>1.5$ [fold change, FC]. The DEMs of both groups their enriched KEGG pathway were analyzed.

Statistical analysis

Statistical analysis was performed using SPSS software (ver. 22.0, IBM Corp. Armonk, NY, USA). One-way ANOVA followed by Duncan's *post hoc* test, was used to compare the cell activity and oxidative stress related indicators among multiple groups. Statistical comparisons between C and P groups were performed using the t -test. $P < 0.05$ indicated significance.

Multivariate statistical analyses, principal component analysis (PCA), relative standard deviation (RSD), Pearson's correlation coefficient, supervised partial least squares discriminant analysis (PLS-DA) and orthogonal partial least squares discriminant analysis (OPLS-DA) were conducted to evaluate data quality control. For the integrated analysis of the proteome and metabolome, the KEGG pathway database was used to identify relevant metabolic processes associated with DEPs and DMs in both groups. Additionally, information regarding their interaction network was also obtained.

RESULTS

Cytotoxicity and cell viability

The morphology and viability of GCs are shown in Fig. 1. Most of the normal adherent GCs (Fig. 1A) were fusiform with good refraction under the microscope. The density of GCs increased with four ng/mL PRL (Fig. 1B), indicating that four ng/mL PRL promoted GCs proliferation. The density of GCs did not decrease significantly with 20 ng/mL PRL (Fig. 1C), indicating that the cytotoxicity was low when the concentration of PRL was 20 ng/mL. The normal spindle-shaped and dead spherical of GCs coexisted when the concentration of PRL was 100 (Fig. 1D) or 500 (Fig. 1E) ng/mL. The number and the density of GCs decreased, and the proportion of GCs transformed from spindle to spherical increased along with the increase of the concentration of PRL, indicating that the toxicity increased with the increase of PRL concentration.

The CCK-8 assay results (Fig. 1F) showed that PRL increased cell viability significantly at the dose of four ng/mL ($P = 0.024$), while 20 ($P = 0.013$), 100 ($P < 0.001$) and 500 ng/mL ($P < 0.001$) PRL obviously inhibited cell viability.

Oxidative stress parameters analysis

The contents of MDA, SOD and T-AOC were shown in Figs. 2A–2C. Compared with the 500 ng/mL group, the content of MDA was repressed in the 0 ($P = 0.006$), 4 ($P = 0.004$), 20 ($P = 0.006$) and 100 ($P = 0.0255$) ng/mL groups, while the content of MDA was higher in the 100 ng/mL group than in the 0 ($P = 0.018$), 4 ($P = 0.006$) and 20 ($P = 0.020$) ng/mL groups, and the content of MDA was elevated in the 0 ($P < 0.001$) and 20 ($P < 0.001$) ng/mL groups compared with the four ng/mL group. The activity of SOD was increased in the 0 ($P = 0.004$), 4 ($P < 0.001$), 20 ($P = 0.004$) and 100 ($P = 0.044$) ng/mL groups

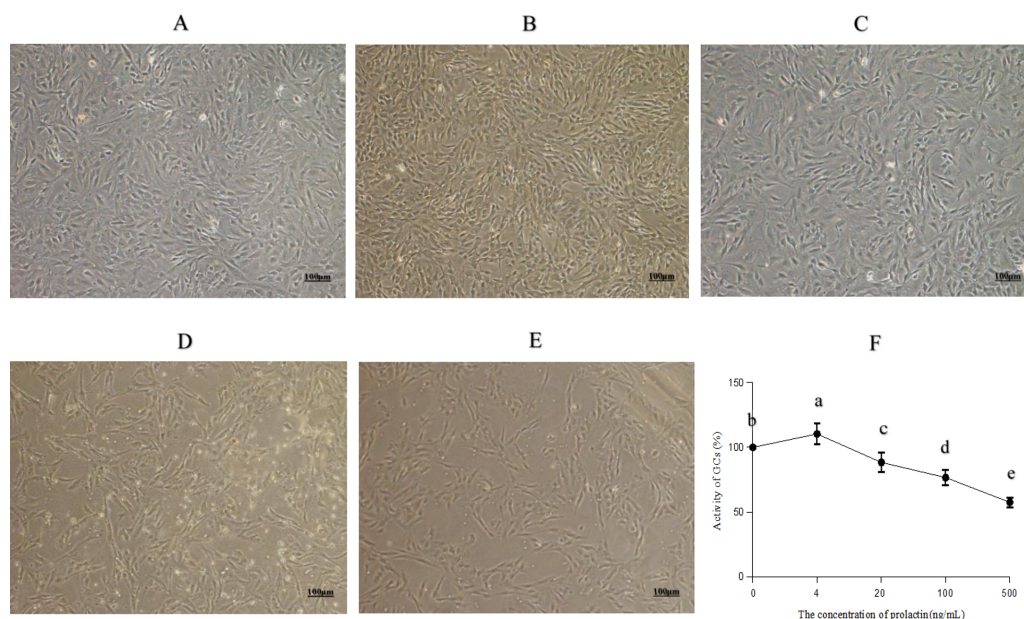


Figure 1 Morphology and activity of ovine granulosa cells (GCs). (A) Morphology of normal GCs (0 ng/mL PRL), (B) morphology of GCs with four ng/mL PRL, (C) morphology of GCs with 20 ng/mL PRL, (D) morphology of GCs with 100 ng/mL PRL, (E) morphology of GCs with 500 ng/mL PRL, and (F) cell activity of granulosa cells. The different lowercase letters indicate significant differences ($P < 0.05$). PRL, Prolactin.

Full-size DOI: [10.7717/peerj.15629/fig-1](https://doi.org/10.7717/peerj.15629/fig-1)

compared with the 500 ng/mL group, while the activity of SOD was lower in the 100 ng/mL group than in the 0 ($P = 0.012$), 4 ($P < 0.001$) and 20 ($P = 0.011$) ng/mL groups, and the activity of SOD was increased in the 0 ($P = 0.002$) and 20 ($P < 0.001$) ng/mL groups compared with the four ng/mL group. Relative to the 500 ng/mL group, the T-AOC was decreased in the 0 ($P = 0.003$), 4 ($P = 0.002$), 20 ($P = 0.015$) and 100 ($P = 0.017$) ng/mL groups, while the T-AOC was lower in the 100 ng/mL group than in the 0 ($P = 0.005$) and 4 ($P = 0.003$) ng/mL groups. The level of ROS was shown in Fig. 2. Intracellular ROS was evaluated by fluorescein isothiocyanate-A (FITC-A). With the increase of PRL concentration, the level of ROS decreased first and then increased. The forward scatter area and FITC-A of ROS were shown in Figs. 2D–2E. Relative to the 500 ng/mL group, the level of ROS was decreased in the 0 ($P < 0.001$), 4 ($P < 0.001$), 20 ($P < 0.001$) and 100 ($P = 0.007$) ng/mL groups, while the ROS was higher in the 100 ng/mL group than in the 0 ($P = 0.002$), 4 ($P = 0.001$) and 20 ($P = 0.002$) ng/mL groups, and the level of ROS was increased in the 0 ($P = 0.021$) and 20 ($P = 0.032$) ng/mL groups compared with the 4 ng/mL group.

Proteomic analysis

Protein identification and the analysis of DEPs

There were 821,838 LC-MS/MS spectra matched to the known spectra, whereas the number of available spectra was 120,505. Overall, 7,552 credible proteins and 85,761 peptides from all GCs samples were detected and quantified by 1% FDR. However, only 7,499 proteins

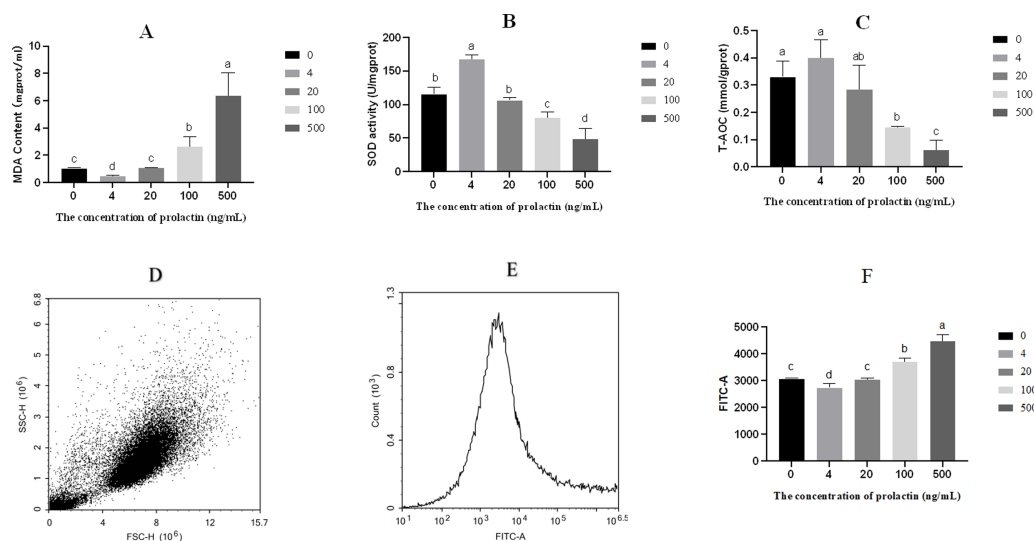


Figure 2 Oxidative stress parameters. (A) The content of MDA, (B) the activity of SOD, (C) T-AOC, (D) forward scatter area of ROS, (E) FITC-A of ROS, (F) the content of ROS. The different lowercase letters indicate significant differences ($P < 0.05$). MDA: Malondialdehyde; SOD: Superoxide Dismutase; T-AOC: Total antioxidant capacity; ROS, Reactive oxygen species.

Full-size [DOI: 10.7717/peerj.15629/fig-2](https://doi.org/10.7717/peerj.15629/fig-2)

could be quantified (Fig. 3A). PCA, RSD and Pearson's Correlation Coefficient were performed to evaluate the reproducibility of protein quantification. The PCA plot (Fig. 3B) indicated that the proteomic analysis was reliable; RSD (Fig. 3C) showed that the whole samples were more repetition, and Pearson's correlation coefficient (Fig. 3D) indicated the samples had a high degree of similarity.

According to the criteria of P value < 0.05 and $FC > 1.2$ or $FC < 0.83$, Relative to the C group, 93 proteins among all credible proteins were significantly downregulated or upregulated in P group. The volcano map and heatmap of the DEPs were shown in Figs. 3E and 3F, respectively. Among the 93 DEPs, P0C276 (UBA52), Q9MZS7 (BCL2L1) and W5QEW6 (MAPK12) were associated with mitophagy. O78747 (MT-ND1) was contacted with reactive oxygen species (ROS). Q9MZS7 (BCL2L1) and W5QEW6 (MAPK12) enriched with functions correlated with apoptosis and NOD-like receptor signaling pathway. P0C276 (UBA52) and W5PQR5 (RPL18) were involved in ribosome. Q9MZS7 (BCL2L1) and W5QEW6 (MAPK12) were closely related to p53 signaling pathway, and 078747 (MT-ND1) in connection with oxidative phosphorylation (Table 2). We found that the DEPs involved in antioxidant related functions were significantly upregulated in the P group. Here, four proteins (UBA52, BCL2L1, MT-ND1 and MAPK12) related to OS were selected for validation (Fig. 4). The results of western blotting verified that these protein expression levels in P group were significantly higher than C group, which consistent with the proteomic findings.

GO functional classification and KEGG pathway analysis of DEPs

In order to obtain in-depth understanding of the biological significance, the enrichment of DEPs according to GO were tested. As a result, 102 GO terms significantly enriched for

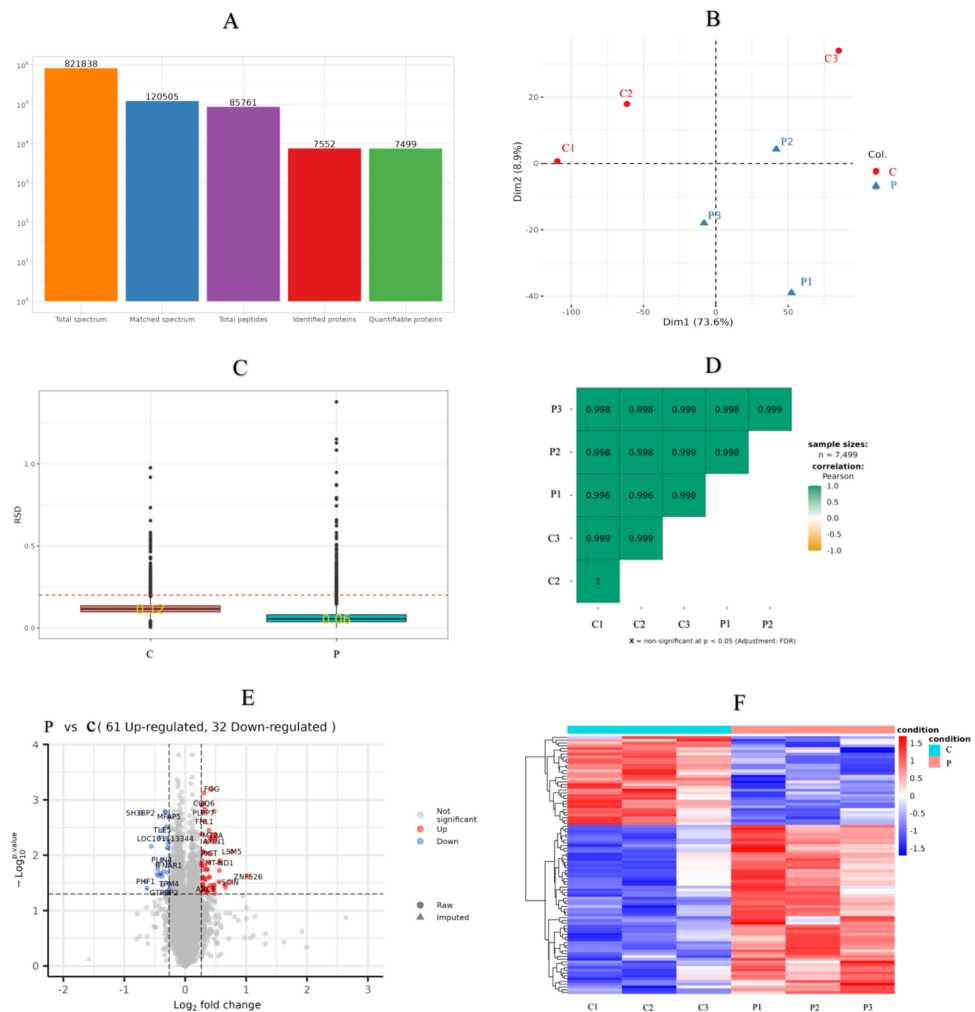


Figure 3 Sample repeatability test and DEPs in the proteomic. (A) An overview of protein identification, (B) PCA score plot exhibiting significant difference between C (control group: 0 ng/mL PRL) and P (500 ng/mL PRL) groups ($n = 6$), (C) relative standard deviation, (D) Pearson's correlation coefficient, (E) volcano plot depicting the DEPs in C and P groups ($n = 6$), and (F) hierarchical clustering of the DEPs between the two groups ($n = 6$). DEPs, differentially expressed proteins. A–F, C: control group (0 ng/mL PRL); P: P group (500 ng/mL PRL).

Full-size [DOI: 10.7717/peerj.15629/fig-3](https://doi.org/10.7717/peerj.15629/fig-3)

Table 2 Differentially expressed proteins induced by high PRL.

Genes	Proteins	Gene ID	P-value
<i>UBA52</i>	P0C276	443296	0.035
<i>MT-ND1</i>	O78747	808249	0.014
<i>BCL2L1</i>	Q9MZS7	443061	0.035
<i>MAPK12</i>	W5QEW6	101115956	0.048
<i>RPL18</i>	W5PQR5	101122808	0.004

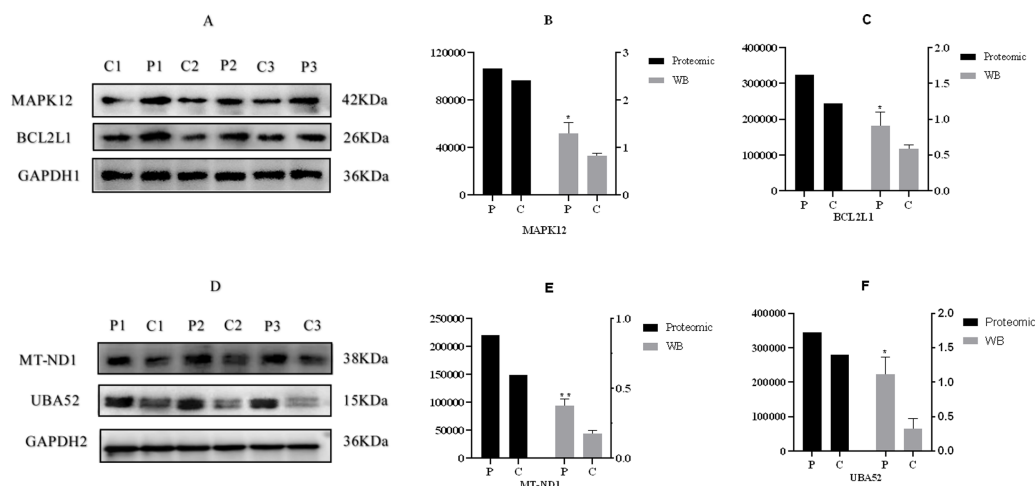


Figure 4 Western blotting validation of proteomic. (A) & (D), Western blotting result, (B), (C), (E) & (F), the expression of four proteins. “*” and “**” indicates $0.01 < P < 0.05$ and $P < 0.01$, respectively. A–F, C: control group (0 ng/mL PRL); P: P group (500 ng/mL PRL). The Western blotting data is referenced on the right Y-axis, while the proteome data is referenced on the left Y-axis.

Full-size [DOI: 10.7717/peerj.15629/fig-4](https://doi.org/10.7717/peerj.15629/fig-4)

DEPs consisted of BP, CC and MF for which the number was 56, 24 and 22, respectively. Several GO terms significantly enriched for DEPs were found and shown in Fig. 5A. Among these pathways, the DEPs were mainly associated with the following BPs: mitochondrial electron transport, NADH to ubiquinone, ATP synthesis coupled electron transport, oxidative phosphorylation, electron transport chain, cellular respiration, regulation of ATPase activity, and RNA catabolic process. The main functional groups of DEPs in CC were nuclear membrane, ribosome and actomyosin, and in MF were actin binding, complement binding and NADH dehydrogenase activity.

Significantly enriched pathways in DEPs were analyzed by the KEGG database. The results revealed that these differently express target proteins were able to be mapped to 53 signaling pathways. Among these signaling pathways, the top 20 regulated pathways ranked based on the P -value were presented in Fig. 5B. The corresponding DEPs were mainly associated with pathways related to the following: mitophagy (animal), oxidative phosphorylation, apoptosis, NF-kappa B signaling pathway, ribosome, p53 signaling pathway, oxidative phosphorylation, NOD-like receptor signaling pathway, and chemical carcinogenesis—reactive oxygen species.

Protein-protein interaction analysis

The STRING database was used to further develop the protein-protein interaction (PPI) networks for DEPs. These interactions include both indirect functional links and direct physical connections.

In Fig. 5C, down-regulated proteins are represented by blue nodes, while up-regulated proteins are represented by red nodes. The P0C276 and W5PQR5 proteins greatly influenced the regulation of ribosome, and the findings revealed that some proteins could not interact with one another directly. However, they still play a role through HPC.

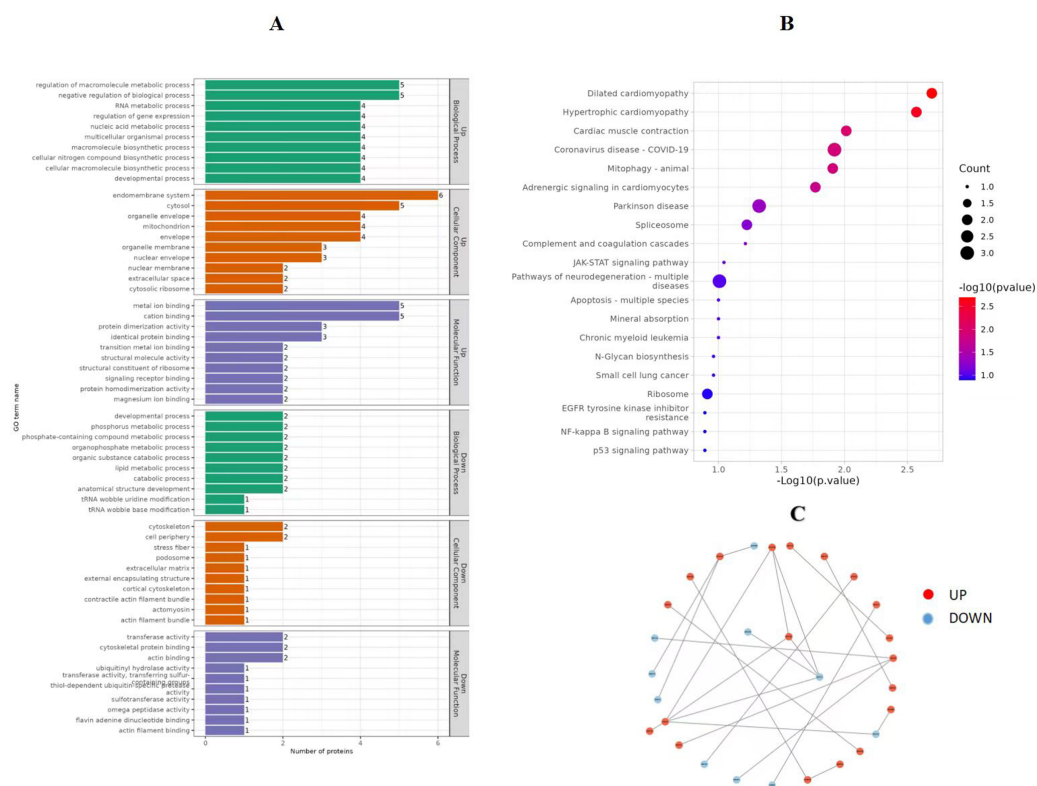


Figure 5 GO function enrichment and KEGG pathways of DEPs (P vs C). (A) GO function enrichment of DEPs, (B) KEGG pathways of DEPs, and (C) protein-protein interaction analysis. GO, Gene Ontology. KEGG, Kyoto Encyclopedia of Genes and Genomes. DEPs, differentially expressed protein. C, control group (0 ng/mL PRL). P, P group (500 ng/mL PRL).

Full-size [DOI: 10.7717/peerj.15629/fig-5](https://doi.org/10.7717/peerj.15629/fig-5)

Metabolomic analysis DEMs identified

The difference in specific metabolites is likely due to the different concentrations of PRL. The metabolites were identified following the treatments with 0 and 500 ng/mL PRL by LC-MS/MS. A total of 1,118 metabolites were identified using the positive ion (POS) mode, and 809 were identified using the negative ion (NEG) mode (Table S1). The OPLS-DA (Figs. 6A and 6B) and PLS-DA (Figs. 6C and 6D) were carried out in two groups to assess the quality control of metabolites. These data suggested that the experimental data were well controlled.

We compared the identified metabolites of ovine ovarian granulosa cells (GCs) from HPC and C groups to elucidate the underlying regulatory mechanism. The results were shown in Fig. 7. In the POS mode (Fig. 7A), 41 DEMs were up-regulated and 15 down-regulated; in the NEG mode (Fig. 7B), 40 DEMs were up-regulated and 38 down-regulated. These DEMs were mainly organic acids, lipids, inorganic alkanes, alcohols, carbohydrates, aldehydes, and ketones at POS and NEG modes. The relative abundance of these DMs was shown in Fig. 7C (POS) and Fig. 7D (NEG).

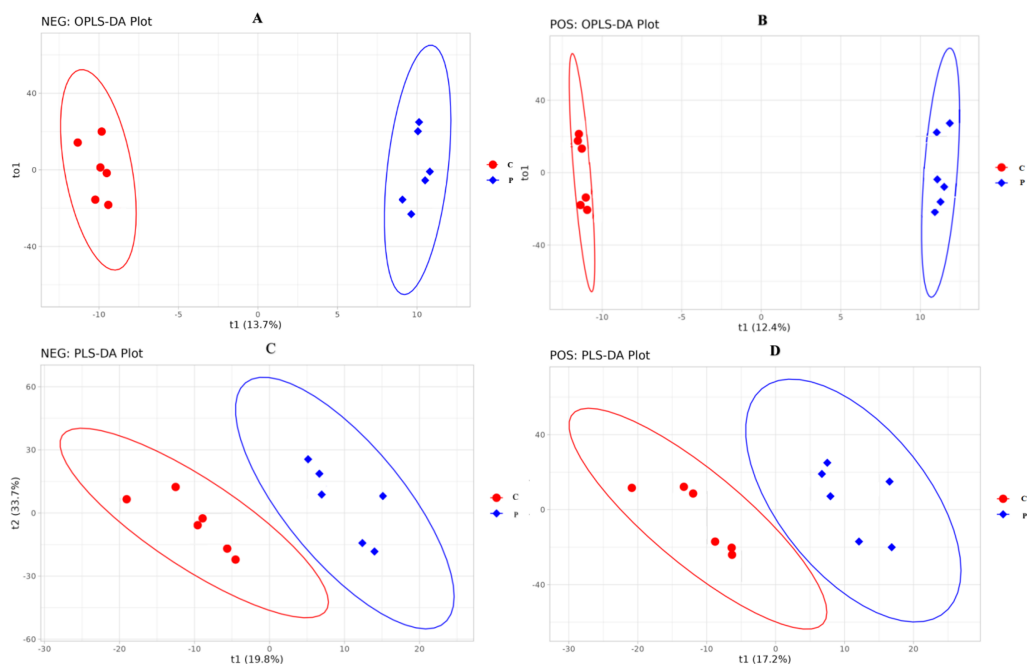


Figure 6 OPLS-DA and PLS-DA score plot of C and P groups (P vs C). NEG, negative ion. POS, positive ion. (A–D), C: Control group (0 ng/mL PRL); P: P group (500 ng/mL PRL).

Full-size [DOI: 10.7717/peerj.15629/fig-6](https://doi.org/10.7717/peerj.15629/fig-6)

Table 3 Differentially expressed metabolites induced by high PRL.

ID	Name	Formula	P-value
POS0391	(R)-Lactate	C ₃ H ₆ O ₃	0.010
POS0646	2-Carboxy-D-arabinitol1-phosphate	C ₆ H ₁₃ O ₁₀ P	0.028
NEG0427	D-Erythrose4-phosphate	C ₄ H ₉ O ₇ P	0.036
NEG0085	6-Phosphogluconic acid	C ₆ H ₁₃ O ₁₀ P	0.028

KEGG pathway analysis of DEMs

The pathway analysis utilised the KEGG database to identify the significantly enriched biochemical processes in DEMs. The results showed that the signaling pathways included 14 pathways at POS mode and 11 pathways at NEG mode. After pathway enrichment analysis, the regulated pathways ranked based on the *P*-value were presented in Fig. 7. The corresponding DEMs at POS mode (Fig. 7E) were mainly associated with pathways related to the following: tryptophan metabolism, cAMP signaling pathway, the pentose phosphate pathway, and purine metabolism. In the NEG mode (Fig. 7F), the DEMs were involved in several KEGG pathways, including purine metabolism, pentose phosphate pathway, and pyrimidine metabolism. Among them, the DEMs enriched in the pentose phosphate pathway were as follows (Table 3): (R)-Lactate and 2-Carboxy-D-arabinitol1-phosphate in POS mode, and D-Erythrose4-phosphate and 6-Phosphogluconic acid in NEG mode.

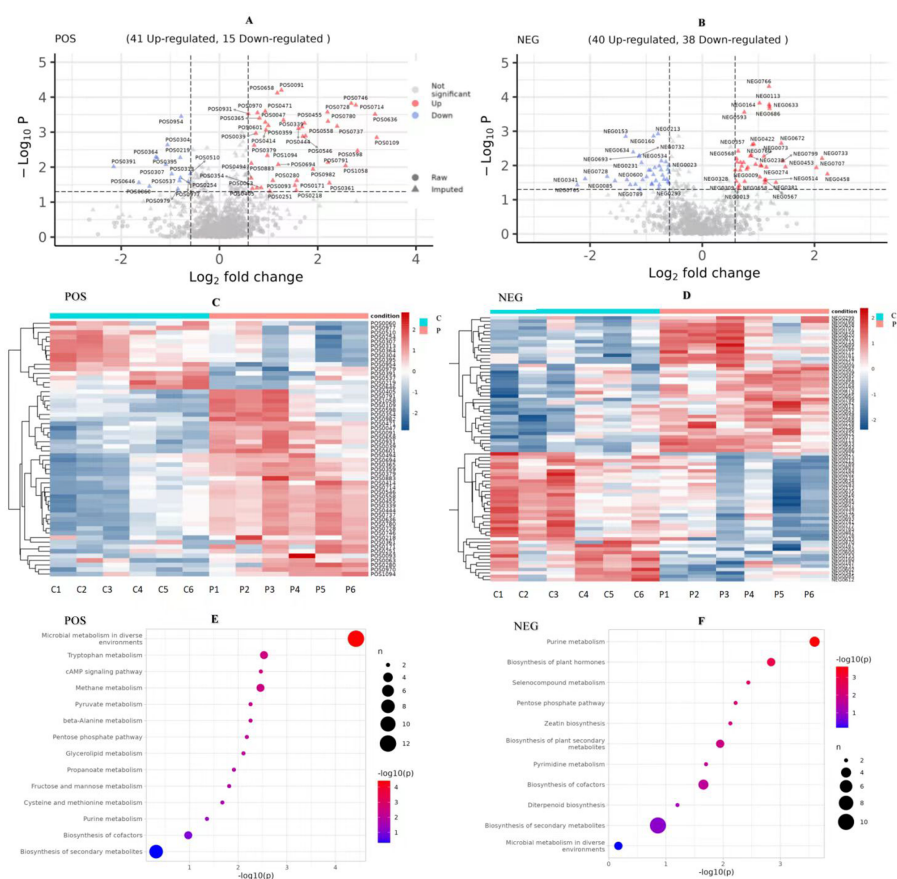


Figure 7 Analysis of metabolomic between C and P groups (P vs C). (A) Volcano map of DEMs at POS mode, (B) volcano map of DEMs at NEG mode, (C) cluster heat map of DEMs at POS mode, (D) cluster heat map of DEMs at NEG mode, (E) KEGG pathways of DEMs at POS mode, and (F) KEGG pathways of DEMs at NEG mode. DEMs, differentially expressed metabolites. POS, positive ion MODE. NEG, negative ion mode. KEGG, Kyoto Encyclopedia of Genes and Genomes. C, control group (0 ng/mL PRL). P, P group (500 ng/mL PRL).

Full-size [DOI: 10.7717/peerj.15629/fig-7](https://doi.org/10.7717/peerj.15629/fig-7)

Integrated omics analysis of proteomics and metabolomics

An integrated analysis based on the aforesaid omics data was conducted to identify the related enriched pathways of the DEPs and DEMs. As a result, Therefore, the pathway information was captured by mapping these DEPs to the KEGG pathway database (Fig. 8). Overall, four enriched KEGG pathways related to OS based on DEPs were obtained, which mainly included mitophagy (animal), apoptosis, ribosome, and chemical carcinogenesis—reactive oxygen species. The metabolomic results showed that the DEMs in the POS and NEG modes were both enriched in the pentose phosphate pathway, and NADPH produced in the pentose phosphate pathway was critical for alleviating ROS-related cell damage.

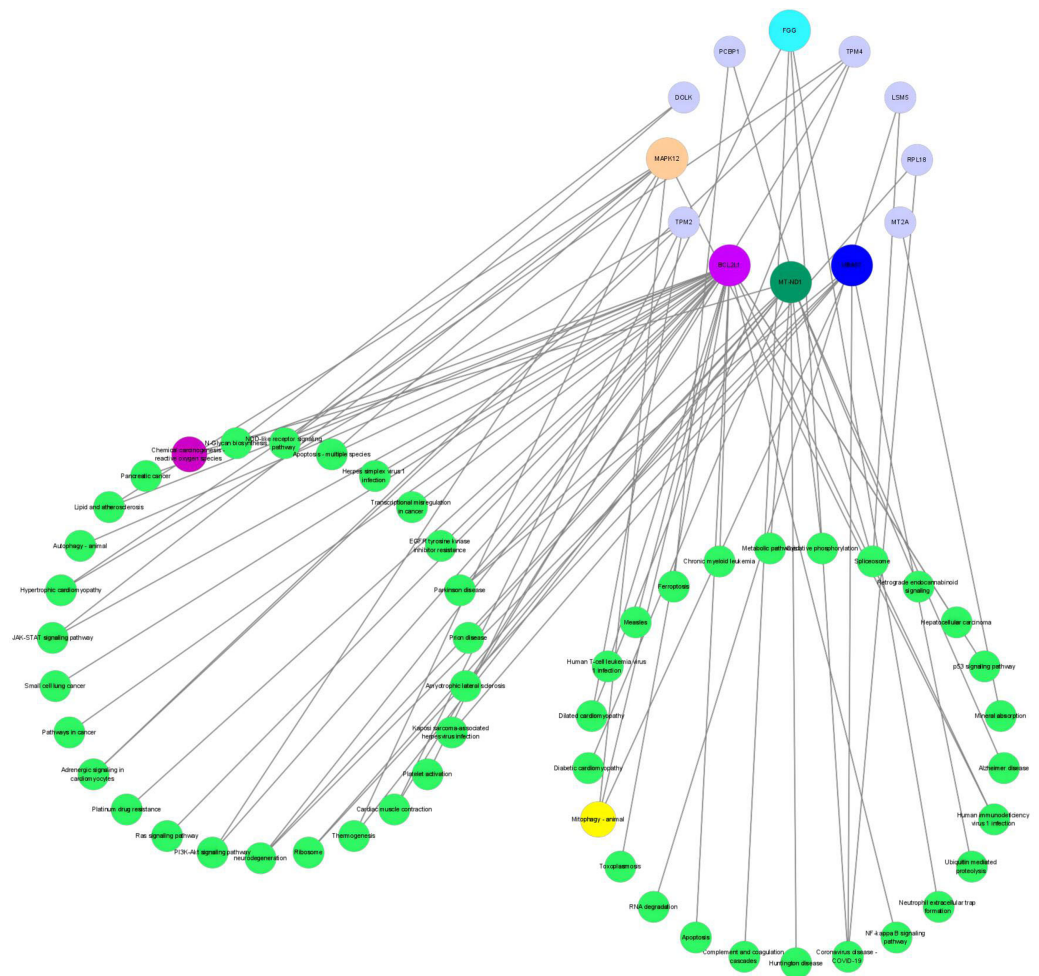


Figure 8 The networks regulation of DEPs. DEPs, Differentially expressed proteins.

Full-size  DOI: [10.7717/peerj.15629/fig-8](https://doi.org/10.7717/peerj.15629/fig-8)

DISCUSSION

The effect of PRL on cytotoxicity and oxidative stress in ovine ovarian GCs

PRL has been reported to be associated with cell proliferation and apoptosis, with low concentration of PRL promoting cell proliferation and high concentration leading to apoptosis (Zhang *et al.*, 2016a; Zhang *et al.*, 2016b). In our study, the low concentration (four ng/mL) of PRL promoted cell proliferation and inhibited cytotoxicity, while HPC showed the opposite effect in ovine ovarian GCs, which was consistent with the previous study. Additionally, PRL has also been reported to play an important role in oxidative-antioxidant balance (Farmer, Lapointe & Cormier, 2017; Rodak *et al.*, 2022). Previous study showed that a moderate dose of PRL promotes the antioxidant capacity of adult RPE 19 human cells by reducing glutathione (Melendez Garcia *et al.*, 2016), suggesting PRL could exert an antioxidant action. However, several studies have discovered that HPC leads to oxidative stress in mammals (Farmer, Lapointe & Cormier, 2017), with an increase in ROS

generation and alterations to antioxidant system components (Rodak et al., 2022), which is consistent with the results of the present study. In our study, the level of ROS in the four ng/mL group was decreased, the content of MDA depressed, and the levels of SOD and T-AOC were increased compared to other groups, but the results of the 500 ng/ml group showed the opposite trend. Previous studies suggested that pathologic conditions produced high ROS levels in ovarian follicles, leading to oxidative stress and extensive GCs damage (Shen et al., 2016; Esfandyari et al., 2021). Therefore, a possible explanation for the ROS increase in the present trial might be due to PRL-induced cytotoxicity in the GCs. However, the detailed mechanism that HPC causes oxidative stress in GCs stills needs further investigation.

Integrated omics analysis of proteomic and metabolomic

Mitochondria are a unique dynamic double membrane-bound organelle (Hagberg et al., 2014) that perform an essential regulatory function in apoptosis (Abate et al., 2020) and ROS production (Protasoni & Zeviani, 2021). When electron transport in the mitochondrial respiratory chain is impaired and decoupled from ATP, which leads to the production of ROS (Sommer et al., 2016). ROS generated by oxidative stress can seriously affect cell development, function and survival while possibly inflicting damage to intracellular macromolecules and mitochondria through various signalling pathways. Mitochondria are important in deciding oocyte developmental competence. GCs around oocytes, on the other hand, can enhance mitochondrial function *via* mitophagy, thereby enhancing oocyte developmental ability (Zhang et al., 2022). Previous studies have shown that the mitochondria from human GCs are involved in oocyte maturation and embryo development (Boucret et al., 2015; Ogino et al., 2016). Moreover, melatonin (Jiang et al., 2021) and FSH (Besnard, Horne & Whitehead, 2001) repressed mitophagy to protect mouse GCs from oxidative damage. Olavarria, Figueroa & Mulero (2012) reported that physiological concentrations of native PRL were able to induce the production of ROS in head kidney leukocytes and macrophages from the teleost fish gilthead seabream and PRL is among the hormones that can impact mitochondrial function and modulate the underlying adaptations to changing bioenergetic and metabolic needs (Alvarez-Delgado, 2022), suggesting that PRL can act on oxidative stress in ovine ovarian GCs through ROS pathway and mitophagy pathway. It is consistent with the results of this study. In this study, we identified the cellular responses in ovine ovarian GCs by analyzing proteomes after handling with 500 ng/mL PRL. The results showed that the ROS pathway and the mitophagy pathway were changed significantly.

In the present study, MT-ND1 enriched in the ROS pathway, UBA52, BCL2L1 and MAPK12 enriched in the mitophagy pathway were screened by proteomics. The study showed that higher expression of MT-ND1 in the recurrent implantation failure (RIF) group compared with the healthy group may be related to increased oxidative stress in the endometrium (Eker et al., 2021). High mitochondrial oxidative phosphorylation (mt- OXPHOS) levels might be generated excessive ROS and have an adverse effect on follicular health (Hoque et al., 2021). Ubiquitin-52 amino acid fusion protein (Uba52) is translated and expressed by Uba52 gene which participates in oxidative stress, ribosome and the

ubiquitin-proteasome pathway (UPP) (Yang & Zhang, 2014). Under hypoxia conditions, ubiquitin protein UBA52 was down-regulated and ubiquitinated through its interaction with apoptosis-inducing factors, resulting in mitosis and abnormal autophagy (Ma et al., 2022). MAPK12 is a key member of the P38 (MAPK) pathway (Cuadrado & Nebreda, 2010). It has been reported that physalin A can induce ROS-mediated apoptosis, and autophagy plays a protective role through the p38 (MAPK)-NFKB/NF-kappaB survival pathway (He et al., 2013). There was also a study which showed that copper-induced oxidative stress will induce protective autophagy through transcriptional regulation of autophagy genes by activation of the MAPK pathway in HeLa cells (Zhong et al., 2014). BCL2L1, as a member of Bcl-2 family, was up-regulated under oxidative stress (Wang et al., 2019) and the expression of *BCL2L1* mRNA levels, encoding for *BCL-xL*, was down-regulated through oxidative stress by dehydration in cortex (Ali et al., 2020). Bcl-2 can induce the necrotic type of death in human coronary artery endothelial cells through oxidative stress (Maslanakova et al., 2016). A study showed that the human adipose-derived mesenchymal stem cells exposure to GC-DNA increased oxidative stress along with the increase of BCL2L1 (Kostyuk et al., 2015). Therefore, differential proteins MT-ND1 enriched in the ROS pathway and UBA52, BCL2L1 as well as MAPK12 enriched in the mitophagy pathway were closely related to oxidative stress.

PRL binding to the prolactin receptor (*PRLR*) exerts pleiotropic biological effects in mammals (Hu, Zhuang & Dufau, 1998). Nie et al. (2021) showed that short *PRLR* regulates the pentose phosphate pathway in human by reducing the expression of two rate-limiting enzymes in pentose phosphate metabolism, G6PD and TKT. In this study, we screened the pentose phosphate pathway by both POS and NEG modes of the metabolomic. Researchers explored that HK2 attenuates cardiac hypertrophy by decreasing ROS accumulation via increased pentose phosphate pathway flux (McCommis et al., 2013). Agarwal et al. (2021) showed that Parkin, a key effector of mitophagy altered in Parkinson's disease, inhibits the pentose phosphate pathway, which creates metabolic and oxidative stress. BCL2L1, an important apoptosis regulating protein, is localized to the outer mitochondrial membrane (Sillars-Hardebol et al., 2012). Data also demonstrated that mitochondrial BCL2L1 is participate in keeping mitochondrial respiratory capacity, and it accumulated under oxidative stress (Stiegler et al., 2013), which is related with glycolytic capacity and balanced by increased pentose phosphate pathway activity (Pfeiffer et al., 2017). Hence, the pentose phosphate pathway can regulate oxidative stress through ROS and mitophagy, which is consistent with our experimental results. In this study, the pentose phosphate pathway was changed significantly in ovine ovarian GCs by analyzing metabolomic after handling with 500 ng/mL PRL.

CONCLUSIONS

1. Low concentration of PRL inhibited cytotoxicity and oxidative stress while high PRL concentration induced cytotoxicity and oxidative stress.
2. High PRL concentration promoted oxidative stress in ovine ovarian GCs by the pentose phosphate pathway through regulating the related proteins MT-ND1 in the ROS pathway, and UBA52, MAPK12 and BCL2L1 in the mitophagy pathway.

ACKNOWLEDGEMENTS

The authors express their gratitude to fellow students in the laboratory for assistance.

ADDITIONAL INFORMATION AND DECLARATIONS

Funding

This research was supported by the China Agriculture Research System (CARS-38) and (CARS-39-23); the Innovative ability training funding project for graduate students supported by the Hebei Provincial Department of Education (CXZZBS2022049). The funders had no role in study design, data collection and analysis, decision to publish, or preparation of the manuscript.

Grant Disclosures

The following grant information was disclosed by the authors:

China Agriculture Research System: CARS-38, CARS-39-23.

Hebei Provincial Department of Education: CXZZBS2022049.

Competing Interests

The authors declare there are no competing interests.

Author Contributions

- Ruochen Yang conceived and designed the experiments, performed the experiments, analyzed the data, prepared figures and/or tables, authored or reviewed drafts of the article, and approved the final draft.
- Shuo Zhang performed the experiments, analyzed the data, authored or reviewed drafts of the article, and approved the final draft.
- Chunhui Duan performed the experiments, analyzed the data, authored or reviewed drafts of the article, and approved the final draft.
- Yunxia Guo analyzed the data, prepared figures and/or tables, and approved the final draft.
- Xinyu Shan analyzed the data, prepared figures and/or tables, and approved the final draft.
- Xinyan Zhang analyzed the data, prepared figures and/or tables, and approved the final draft.
- Sicong Yue analyzed the data, prepared figures and/or tables, and approved the final draft.
- Yingjie Zhang conceived and designed the experiments, analyzed the data, authored or reviewed drafts of the article, and approved the final draft.
- Yueqin Liu analyzed the data, authored or reviewed drafts of the article, and approved the final draft.

Data Availability

The following information was supplied regarding data availability:

The mass spectrometry proteomics data are available at the ProteomeXchange Consortium via the iProX partner repository: [PXD037645](https://doi.org/10.1093/bioinformatics/btad008).

The raw data are available in the [Supplemental Files](#).

Supplemental Information

Supplemental information for this article can be found online at <http://dx.doi.org/10.7717/peerj.15629#supplemental-information>.

REFERENCES

- Abate M, Festa A, Falco M, Lombardi A, Luce A, Grimaldi A, Zappavigna S, Sperlongano P, Irace C, Caraglia M, Misso G. 2020. Mitochondria as playmakers of apoptosis, autophagy and senescence. *Seminars in Cell & Developmental Biology* 98:139–153 DOI [10.1016/j.semcdb.2019.05.022](https://doi.org/10.1016/j.semcdb.2019.05.022).
- Abedelahi A, Abdelahi A, Salehnia M, Allameh AA, Davoodi D. 2010. Sodium selenite improves the *in vitro* follicular development by reducing the reactive oxygen species level and increasing the total antioxidant capacity and glutathione peroxidase activity. *Human Reproduction* 25(4):977–985 DOI [10.1093/humrep/deq002](https://doi.org/10.1093/humrep/deq002).
- Agarwal E, Goldman AR, Tang HY, Kossenkov AV, Ghosh JC, Languino LR, Vaira V, Speicher DW, Altieri DC. 2021. A cancer ubiquitome landscape identifies metabolic reprogramming as target of Parkin tumor suppression. *Science Advances* 7(35):eabg7287 DOI [10.1126/sciadv.abg7287](https://doi.org/10.1126/sciadv.abg7287).
- Ali MA, Abu Damir H, Ali OM, Amir N, Tariq S, Greenwood MP, Lin P, Gillard B, Murphy D, Adem A. 2020. The effect of long-term dehydration and subsequent rehydration on markers of inflammation, oxidative stress and apoptosis in the camel kidney. *BMC Veterinary Research* 16(1):458 DOI [10.1186/s12917-020-02628-5](https://doi.org/10.1186/s12917-020-02628-5).
- Alvarez-Delgado C. 2022. The role of mitochondria and mitochondrial hormone receptors on the bioenergetic adaptations to lactation. *Molecular and Cellular Endocrinology* 551:111661 DOI [10.1016/j.mce.2022.111661](https://doi.org/10.1016/j.mce.2022.111661).
- Besnard N, Horne EAL, Whitehead SA. 2001. Prolactin and lipopolysaccharide treatment increased apoptosis and atresia in rat ovarian follicles. *Acta Physiologica Scandinavica* 172(1):17–25 DOI [10.1046/j.1365-201X.2001.00813.x](https://doi.org/10.1046/j.1365-201X.2001.00813.x).
- Boucret L, De la Barca JMC, Moriniere C, Desquirit V, Ferre-L'Hotellier V, Descamps P, Marcaillou C, Reynier P, Procaccio V, May-Panloup P. 2015. Relationship between diminished ovarian reserve and mitochondrial biogenesis in cumulus cells. *Human Reproduction* 30(7):1653–1664 DOI [10.1093/humrep/dev114](https://doi.org/10.1093/humrep/dev114).
- Caja G, Elhadi A, Such X, Salama AAK. 2020. Suppression of prolactin and reduction of milk secretion by effect of cabergoline in lactating dairy ewes. *Journal of Dairy Science* 103(12):12033–12044 DOI [10.3168/jds.2019-18087](https://doi.org/10.3168/jds.2019-18087).
- Chen HX, Fu J, Huang W. 2016. Dopamine agonists for preventing future miscarriage in women with idiopathic hyperprolactinemia and recurrent miscarriage history. *Cochrane Database of Systematic Reviews* 7(7):CD008883 DOI [10.1002/14651858.CD008883.pub2](https://doi.org/10.1002/14651858.CD008883.pub2).

- Cuadrado A, Nebreda AR. 2010.** Mechanisms and functions of p38 MAPK signalling. *Biochemical Journal* **429**:403–417 DOI [10.1042/BJ20100323](https://doi.org/10.1042/BJ20100323).
- Drejza MA, Rylewicz K, Majcherek E, Gross-Tyrkin K, Mizgier M, Plagens-Rotman K, Wojcik M, Panecka-Mysza K, Pisarska-Krawczyk M, Kedzia W, Jarzabek-Bielecka G. 2022.** Markers of oxidative stress in obstetrics and gynaecology—a systematic literature review. *Antioxidants* **11**(8):1477 DOI [10.3390/antiox11081477](https://doi.org/10.3390/antiox11081477).
- Eker C, Basdas R, Balci BK, Bastu E, Gunel T. 2021.** The genomic analysis of endometrial mitochondrial DNA copy number variation on recurrent implantation failure. *Journal of Gynecology Obstetrics and Human Reproduction* **50**(2):101945 DOI [10.1016/j.jogoh.2020.101945](https://doi.org/10.1016/j.jogoh.2020.101945).
- Esfandyari S, Aleyasin A, Noroozi Z, Taheri M, Khodarahmian M, Eslami M, Rashidi Z, Amidi F. 2021.** The protective effect of sulforaphane against oxidative stress through activation of NRF2/ARE pathway in human granulosa cells. *Cell Journal* **23**(6):692–700 DOI [10.22074/cellj.2021.7393](https://doi.org/10.22074/cellj.2021.7393).
- Farmer C, Lapointe J, Cormier I. 2017.** Providing the plant extract silymarin to lactating sows: effects on litter performance and oxidative stress in sows. *Animal* **11**(3):405–410 DOI [10.1017/S1751731116001919](https://doi.org/10.1017/S1751731116001919).
- Gu F, Hu ZZ, Li YX, Sun LL. 1993.** Discussion on the level of prolactin in women's follicular fluid and its relationship with estradiol and progesterone. *Tianjin Medical Journal* **01**:35–37 (in Chinese).
- Hagberg H, Mallard C, Rousset CI, Thornton C. 2014.** Mitochondria: hub of injury responses in the developing brain. *Lancet Neurology* **13**(2):217–232 DOI [10.1016/S1474-4422\(13\)70261-8](https://doi.org/10.1016/S1474-4422(13)70261-8).
- He LL, Li JJ, Shi L, Zhao QY, Wu ZG, Zeng SH, Li YQ, Zhang W, Wang FD, Zhang S. 2021.** Exogenous metabolites spray, which identified from metabolomics analysis and transcriptomic analysis, can improve salt tolerance of Chinese cabbages (*Brassica rapa* L.ssp *pekinensis*)*. *Journal of Plant Interactions* **16**(1):452–461.
- He H, Zang LH, Feng YS, Chen LX, Kang N, Tashiro SI, Onodera S, Qiu F, Ikejima T. 2013.** Physalin A induces apoptosis via p53-Noxa-mediated ROS generation, and autophagy plays a protective role against apoptosis through p38-NF-kappa B survival pathway in A375-S2 cells. *Journal of Ethnopharmacology* **148**(2):544–555 DOI [10.1016/j.jep.2013.04.051](https://doi.org/10.1016/j.jep.2013.04.051).
- Hennet ML, Yu HY, Combelles CMH. 2013.** Follicular fluid hydrogen peroxide and lipid hydroperoxide in bovine antral follicles of various size, atresia, and dominance status. *Journal of Assisted Reproduction and Genetics* **30**(3):333–340 DOI [10.1007/s10815-012-9925-5](https://doi.org/10.1007/s10815-012-9925-5).
- Henriques PC, Aquino NSS, Campideli-Santana AC, Silva JF, Araujo-Lopes R, Franci CR, Coimbra CC, Szawka RE. 2022.** Hypothalamic expression of estrogen receptor isoforms underlies estradiol control of luteinizing hormone in female rats. *Endocrinology* **163**(8):bqac101 DOI [10.1210/endo/bqac101](https://doi.org/10.1210/endo/bqac101).
- Hilali N, Vural M, Camuzcuoglu H, Camuzcuoglu A, Aksoy N. 2013.** Increased prolidase activity and oxidative stress in PCOS. *Clinical Endocrinology* **79**(1):105–110 DOI [10.1111/cen.12110](https://doi.org/10.1111/cen.12110).

- Hoque SAM, Umehara T, Kawai T, Shimada M. 2021.** Adverse effect of superoxide-induced mitochondrial damage in granulosa cells on follicular development in mouse ovaries. *Free Radical Biology and Medicine* **163**:344–355
DOI [10.1016/j.freeradbiomed.2020.12.434](https://doi.org/10.1016/j.freeradbiomed.2020.12.434).
- Hu ZZ, Zhuang L, Dufau ML. 1998.** Prolactin receptor gene diversity: structure and regulation. *Trends in Endocrinology and Metabolism* **9**(3):94–102
DOI [10.1016/S1043-2760\(98\)00027-7](https://doi.org/10.1016/S1043-2760(98)00027-7).
- Jiang Y, Shen M, Chen Y, Wei Y, Tao J, Liu H. 2021.** Melatonin represses mitophagy to protect mouse granulosa cells from oxidative damage. *Biomolecules* **11**(7):968
DOI [10.3390/biom11070968](https://doi.org/10.3390/biom11070968).
- Kamel MA, Zabel G, Bernart W, Neulen J, Breckwoldt M. 1994.** Comparison between prolactin, gonadotrophins and steroid hormones in serum and follicular fluid after stimulation with gonadotrophin-releasing hormone agonists and human menopausal gonadotrophin for an *in-vitro* fertilization programme. *Human Reproduction* **9**(10):1803–1806 DOI [10.1093/oxfordjournals.humrep.a138338](https://doi.org/10.1093/oxfordjournals.humrep.a138338).
- Kostyuk S, Smirnova T, Kameneva L, Porokhovnik L, Speranskij A, Ershova E, Stukalov S, Izevskaya V, Veiko N. 2015.** GC-rich extracellular DNA induces oxidative stress, double-strand DNA breaks, and DNA damage response in human adipose-derived mesenchymal stem cells. *Oxidative Medicine and Cellular Longevity* **2015**:782123 DOI [10.1155/2015/782123](https://doi.org/10.1155/2015/782123).
- Lai QH, Xiang WP, Li Q, Zhang HW, Li YF, Zhu GJ, Xiong CL, Jin L. 2018.** Oxidative stress in granulosa cells contributes to poor oocyte quality and IVF-ET outcomes in women with polycystic ovary syndrome. *Frontiers of Medicine* **12**(5):518–524
DOI [10.1007/s11684-017-0575-y](https://doi.org/10.1007/s11684-017-0575-y).
- Li L, Wu J, Luo M, Sun Y, Wang G. 2016.** The effect of heat stress on gene expression, synthesis of steroids, and apoptosis in bovine granulosa cells. *Cell Stress & Chaperones* **21**(3):467–475 DOI [10.1007/s12192-016-0673-9](https://doi.org/10.1007/s12192-016-0673-9).
- Lu YR, Kuang AK, Ding T, Chen JL. 1983.** Clinical study of prolactin. *Shanghai Medical Journal* (12) (in Chinese).
- Ma C, Wang X, He S, Zhang L, Bai J, Qu L, Qi J, Zheng X, Zhu X, Mei J, Guan X, Yuan H, Zhu D. 2022.** Ubiquitinated AIF is a major mediator of hypoxia-induced mitochondrial dysfunction and pulmonary artery smooth muscle cell proliferation. *Cell and Bioscience* **12**(1):9 DOI [10.1186/s13578-022-00744-3](https://doi.org/10.1186/s13578-022-00744-3).
- Malaguarnera L, Pilastro MR, Quan S, Ghattas MH, Yang L, Mezentsev AV, Kushida TT, Abraham NG, Kappas A. 2002.** Significance of heme oxygenase in prolactin-mediated cell proliferation and angiogenesis in human endothelial cells. *International Journal of Molecular Medicine* **10**(4):433–440.
- Maslanakova M, Balogova L, Miskovsky P, Tkacova R, Stroffekova K. 2016.** Anti- and pro-apoptotic Bcl2 proteins distribution and metabolic profile in human coronary aorta endothelial cells before and after HypPDT. *Cell Biochemistry and Biophysics* **74**(3):435–447 DOI [10.1007/s12013-016-0740-y](https://doi.org/10.1007/s12013-016-0740-y).
- Mavoungou E, Bouyou-Akotet MK, Kreamsner PG. 2005.** Effects of prolactin and cortisol on natural killer (NK) cell surface expression and function of human natural

- cytotoxicity receptors (NKp46, NKp44 and NKp30). *Clinical and Experimental Immunology* **139**(2):287–296 DOI [10.1111/j.1365-2249.2004.02686.x](https://doi.org/10.1111/j.1365-2249.2004.02686.x).
- McCommis KS, Douglas DL, Krenz M, Baines CP. 2013.** Cardiac-specific Hexokinase 2 overexpression attenuates hypertrophy by increasing pentose phosphate pathway flux. *Journal of the American Heart Association* **2**(6):e000355 DOI [10.1161/JAHA.113.000355](https://doi.org/10.1161/JAHA.113.000355).
- Melendez Garcia R, Zamarripa DA, Arnold E, Ruiz-Herrera X, Imm RN, Cruz GB, Adan N, Binart N, Riesgo-Escovar J, Goffin V. 2016.** Prolactin protects retinal pigment epithelium by inhibiting sirtuin 2-dependent cell death. *Ebiomedicine* **7**:35–49 DOI [10.1016/j.ebiom.2016.03.048](https://doi.org/10.1016/j.ebiom.2016.03.048).
- Melmed S, Casanueva FF, Hoffman AR, Kleinberg DL, Montori VM, Schlechte JA, Wass JAH. 2011.** Diagnosis and treatment of hyperprolactinemia: an endocrine society clinical practice guideline. *Journal of Clinical Endocrinology & Metabolism* **96**(2):273–288 DOI [10.1210/jc.2010-1692](https://doi.org/10.1210/jc.2010-1692).
- Meniri M, Evans E, Thompson FJ, Marshall HH, Nichols HJ, Lewis G, Holt L, Davey E, Mitchell C, Johnstone RA. 2022.** Untangling the oxidative cost of reproduction: an analysis in wild banded mongooses. *Ecology and Evolution* **12**(3):e8644 DOI [10.1002/ece3.8644](https://doi.org/10.1002/ece3.8644).
- Mitchell C, Johnston RA. 2022.** Untangling the oxidative cost of reproduction: an analysis in wild banded mongooses. *Ecology and Evolution* **12**(3):e8644 DOI [10.1002/ece3.8644](https://doi.org/10.1002/ece3.8644).
- Mohammadi M. 2019.** Oxidative stress and polycystic ovary syndrome: a brief review. *International Journal of Preventive Medicine* **10**:86–86 DOI [10.4103/ijpvm.IJPVM-576-17](https://doi.org/10.4103/ijpvm.IJPVM-576-17).
- Neradugomma NK, Subramaniam D, Tawfik OW. 2014.** Prolactin signaling enhances colon cancer stemness by modulating Notch signaling in a Jak2-STAT3/ERK manner. *Carcinogenesis* **35**(4):795–806 DOI [10.1093/carcin/bgt379](https://doi.org/10.1093/carcin/bgt379).
- Nie H, Huang PQ, Jiang SH, Yang Q, Hu LP, Yang XM, Li J, Wang YH, Li Q, Zhang YF, Zhu L, Zhang YL, Yu Y, Xiao GG, Sun YW, Ji J, Zhang ZG. 2021.** The short isoform of PRLR suppresses the pentose phosphate pathway and nucleotide synthesis through the NEK9-Hippo axis in pancreatic cancer. *Theranostics* **11**(8):3898–3915 DOI [10.7150/thno.51712](https://doi.org/10.7150/thno.51712).
- Ogino M, Tsubamoto H, Sakata K, Oohama N, Hayakawa H, Kojima T, Shigeta M, Shibahara H. 2016.** Mitochondrial DNA copy number in cumulus cells is a strong predictor of obtaining good-quality embryos after IVF. *Journal of Assisted Reproduction and Genetics* **33**(3):367–371 DOI [10.1007/s10815-015-0621-0](https://doi.org/10.1007/s10815-015-0621-0).
- Olavarria VH, Figueroa JE, Mulero V. 2012.** Prolactin-induced activation of phagocyte NADPH oxidase in the teleost fish gilthead seabream involves the phosphorylation of p47phox by protein kinase C. *Developmental and Comparative Immunology* **36**(1):216–221 DOI [10.1016/j.dci.2011.08.004](https://doi.org/10.1016/j.dci.2011.08.004).
- Parraguez VH, Urquieta B, Perez L, Castellaro G, De los Reyes M, Torres-Rovira L, Aguado-Martinez A, Astiz S, Gonzalez-Bulnes A. 2013.** Fertility in a high-altitude environment is compromised by luteal dysfunction: the relative roles

- of hypoxia and oxidative stress. *Reproductive Biology and Endocrinology* **11**:24 DOI [10.1186/1477-7827-11-24](https://doi.org/10.1186/1477-7827-11-24).
- Pfeiffer A, Schneider J, Bueno D, Dolga A, Voss TD, Lewerenz J, Wuellner V, Methner A.** 2017. Bcl-x(L) knockout attenuates mitochondrial respiration and causes oxidative stress that is compensated by pentose phosphate pathway activity. *Free Radical Biology and Medicine* **112**:350–359 DOI [10.1016/j.freeradbiomed.2017.08.007](https://doi.org/10.1016/j.freeradbiomed.2017.08.007).
- Protasoni M, Zeviani M.** 2021. Mitochondrial structure and bioenergetics in normal and disease conditions. *International Journal of Molecular Sciences* **22**(2):586 DOI [10.3390/ijms22020586](https://doi.org/10.3390/ijms22020586).
- Rodak K, Kokot I, Kryla A, Kratz EM.** 2022. The examination of the influence of caffeinated coffee consumption on the concentrations of serum prolactin and selected parameters of the oxidative-antioxidant balance in young adults: a preliminary report. *Oxidative Medicine and Cellular Longevity* **2022**:1735204–1735204 DOI [10.1155/2022/1735204](https://doi.org/10.1155/2022/1735204).
- Schieber M, Chandel NS.** 2014. ROS function in redox signaling and oxidative stress. *Current Biology* **24**(10):R453–R462 DOI [10.1016/j.cub.2014.03.034](https://doi.org/10.1016/j.cub.2014.03.034).
- Shen M, Jiang Y, Guan Z, Cao Y, Sun SC, Liu H.** 2016. FSH protects mouse granulosa cells from oxidative damage by repressing mitophagy. *Scientific Reports* **6**:38090 DOI [10.1038/srep38090](https://doi.org/10.1038/srep38090).
- Sillars-Hardebol AH, Carvalho B, Belien JAM, De Wit M, Delis-van Diemen PM, Tijssen M, Van de Wiel MA, Ponten F, Fijneman RJA, Meijer GA.** 2012. BCL2L1 has a functional role in colorectal cancer and its protein expression is associated with chromosome 20q gain. *Journal of Pathology* **226**(3):442–450 DOI [10.1002/path.2983](https://doi.org/10.1002/path.2983).
- Sommer S, Leistner M, Aleksic I, Schimmer C, Alhussini K, Kanofsky P, Leyh RG, Sommer SP.** 2016. Impact of levosimendan and ischaemia-reperfusion injury on myocardial subsarcolemmal mitochondrial respiratory chain, mitochondrial membrane potential, Ca²⁺ cycling and ATP synthesis(aEuro). *European Journal of Cardio-Thoracic Surgery* **49**(2):e54–e62 DOI [10.1093/ejcts/ezv397](https://doi.org/10.1093/ejcts/ezv397).
- Stiegler P, Sereinigg M, Puntschart A, Bradatsch A, Seifert-Held T, Wiederstein-Grasser I, Leber B, Stadlmeyer E, Dandachi N, Zelzer S, Iberer F, Stadlbauer V.** 2013. Oxidative stress and apoptosis in a pig model of brain death (BD) and living donation (LD). *Journal of Translational Medicine* **11**:244 DOI [10.1186/1479-5876-11-244](https://doi.org/10.1186/1479-5876-11-244).
- Stier A, Reichert S, Masemin S, Bize P, Criscuolo F.** 2012. Constraint and cost of oxidative stress on reproduction: correlative evidence in laboratory mice and review of the literature. *Frontiers in Zoology* **9**:37 DOI [10.1186/1742-9994-9-37](https://doi.org/10.1186/1742-9994-9-37).
- Thebanlt S.** 2017. Potential mechanisms behind the antioxidant actions of prolactin in the retina. *Experimental Eye Research* **160**:56–61 DOI [10.1016/j.exer.2017.03.014](https://doi.org/10.1016/j.exer.2017.03.014).
- Troiano G, Perrone D, Dioguardi M, Buonavogli A, Arrdito F, Muzio LL.** 2018. *In vitro* evaluation of the cytotoxic activity of three epoxy resin-based endodontic sealers. *Dental Materials Journal* **37**(3):374–378 DOI [10.4012/dmj.2017-148](https://doi.org/10.4012/dmj.2017-148).

- Veena BS, Upadhya S, Adiga SK, Pratap KN. 2008.** Evaluation of oxidative stress, antioxidants and prolactin in infertile women. *Indian Journal of Clinical Biochemistry* 23(2):186–90 DOI 10.1007/s12291-008-0041-3.
- Vilar L, Freitas MC, Naves LA, Casulari LA, Azevedo M, Montenegro R, Barros AI, Faria M, Nascimento GC, Lirna JG. 2008.** Diagnosis and management of hyperprolactinemia: results of a Brazilian multicenter study with 1234 patients. *Journal of Endocrinological Investigation* 31(5):436–444 DOI 10.1007/BF03346388.
- Wang Y, Duan H, Liu X, Min Z, Li D. 2019.** Studies of relationship between oxidative stress-induced autophagy and cryptorchidism or teratozoospermia. *Life Sciences Research* 23(4):281–289.
- Yang X, Zhang L. 2014.** Ubiquitin-52 ribosome fusion proteins: an early biomarker of diabetic nephropathy. *Chinese Journal of Nephrology Dialysis Transplantation* 23(2):176–178.
- Yao XY, Xiao SY, Zhou LY. 2021.** Integrative proteomic and metabolomic analyses reveal the mechanism by which bismuth enables eradication. *Helicobacter* 26(6):e12846 DOI 10.1111/hel.12846.
- Yuan SC, Wen JY, Cheng J, Shen W, Zhou S, Yan W, Shen L, Luo AY, Wang SX. 2016.** Age-associated up-regulation of EGR1 promotes granulosa cell apoptosis during follicle atresia in mice through the NF- κ B pathway. *Cell Cycle* 15(21):2895–2905 DOI 10.1080/15384101.2016.1208873.
- Zhang H, Wang C, Li X, Zhang Y. 2016b.** Effects of pterostilbene on treating hyperprolactinemia and related mechanisms. *American Journal of Translational Research* 8(7):3049–3055 DOI 10.1046/j.1365-201X.2001.00813.x.
- Zhang JQ, Gao BW, Wang J, Ren QL, Chen JF, Ma Q, Zhang ZJ, Xing BS. 2016a.** Critical role of FoxO1 in granulosa cell apoptosis caused by oxidative stress and protective effects of grape seed procyanidin B2. *Oxidative Medicine and Cellular Longevity* 2016:6147345 DOI 10.1155/2016/6147345.
- Zhang X, Chen Y, Li H, Chen B, Liu Z, Wu G, Li C, Li R, Cao Y, Zhou J, Shen M, Liu H, Tao J. 2022.** Sulforaphane acts through NFE2L2 to prevent hypoxia-induced apoptosis in porcine granulosa cells via activating antioxidant defenses and mitophagy. *Journal of Agricultural and Food Chemistry* 70(26):8097–8110 DOI 10.1021/acs.jafc.2c01978.
- Zhong W, Zhu H, Sheng F, Tian Y, Zhou J, Chen Y, Li S, Lin J. 2014.** Activation of the MAPK11/12/13/14 (p38 MAPK) pathway regulates the transcription of autophagy genes in response to oxidative stress induced by a novel copper complex in HeLa cells. *Autophagy* 10(7):1285–1300 DOI 10.4161/autophagy.28789.